An efficient pathway to the elaboration of glassy amphiphilic ester based hydroxyethyl cellulose and ionic liquids

Achalhi Nafea, El Ouardi Youssef, El Yousfi Ridouan, Lamsayah Morad, El Barkany Soufian, Laatikainen Katri, El Idrissi Abderrahmane

DOI: 10.1007/s10570-022-04988-7

An efficient pathway to the elaboration of glassy amphiphilic ester based hydroxyethyl cellulose and ionic liquids.

Nafea Achalhi*[a], Youssef El Ouardi*[b], ridouan El yousfi [a], Morad Lamsayah [a], Soufian El Barkany[c], Katri Laatikainen[b], Abderrahmane El Idrissi*[a].

[a]*Laboratory of Applied Chemistry and Environment (LCAE-URAC18), Faculty of Sciences, Mohamed1[st]University, 60000 Oujda, Morocco*
[b]*Lappeenranta-Lahti University of Technology LUT, school of Engineering Science, Department of Separation science, Yliopistonkatu 34 FI-53850 Lappeenranta, Finland.*
[c]*Laboratory of Molecular Chemistry, Materials and Environment (LMCME), Department of Chemistry, Faculty Multidisciplinary Nador, Mohamed 1st University, P. B. 300, Nador 62700, Morocco.*

**Corresponding authors. E-mail adresses : ab.elidrissi@yahoo.fr (El idrissi abderrahmane), achalhi.nafea@ump.ac.ma (Achalhi Nafea), youssef.el.ouardi@lut.fi (El ouardi youssef).*

Abstract:

Hydroxyethyl cellulose (HEC) is considered one of the most important hydro-soluble cellulose derivatives, thanks to its biocompatibility and biodegradability profile. In this work, a facile synthesis methodology was developed to graft ionic liquids onto the HEC ester. Firstly, a low T_g (glass transition temperature) glassy brominated hydrophobic ester based on HEC was prepared. By regioselective nucleophilic substitution of bromine with imidazole and pyridine derivatives, HEC-ILs (Ionic liquids) with a high DS (degree of substitution) were elaborated in a second step. The synthesized HEC-ILs were characterized by nuclear magnetic resonance (^{1}H ,^{13}C NMR), elemental analysis (CHNO), Fourier transform infrared spectroscopy- Attenuated total reflection (FTIR-ATR), x-ray diffraction (XRD), thermogravimetric analysis (TGA), differential scanning calorimetry (DSC) and scanning electron microscopy (SEM). Zeta potential was used to verify the presence of permanent positive charge. Contact angle measurements were exploited to follow the reorganization of the surface of HEC-ILs in contact with water. A theoretical study was carried out to investigate the intra- and intermolecular interactions of polymer chains. The prepared cationic HEC derivatives have attractive properties such as their amphiphilic and glassy character, solubility in water, and a permanent positive charge. Such properties open a wide range of applications in the field of drug delivery and the complexation of anionic molecules.

Keywords: *hydroxyethyl cellulose, Ionic liquids, HEC glassy ester, contact angle, dispersion.*

Introduction:

Many scientific studies have been conducted in order to develop biomaterials and replace synthetic materials that are of non-renewable resources (Tschan et al. 2012; Zhu et al. 2016; Poulopoulou et al. 2018). This will eventually lead to a decrease in the production of synthetic polymers which have consequent societal problems because of their ubiquity in everyday life (packaging, furniture, containers, electronics, etc.) (Joubert et al. 2015). Among the most abundant biopolymers in nature, we find cellulose and its derivatives, starch, proteins and chitosan (Klemm et al. 2005). From a structural point of view, cellulose is a syndiotactic biopolymer of anhydroglucose units (AGU) connected by (1,4) β -glycosidic bonds (Heinze. 2015). Moreover, the importance of this material lies in its interesting physicochemical properties and its attractive advantages such as biocompatibility, biodegradability and non-toxicity (Fu et al. 2019; Shojaeiarani et al. 2019). However, one of the main drawbacks of cellulose is its high degree of crystallinity and insolubility in both organic and aqueous solvents, which limits its industrial uses. To solve this problem, various processes of cellulose modification have been developed under appropriate conditions disrupting the hydrogen bonding network and leading to an improvement of its solubility, especially solubility in water.

HEC is one of the most important commercial water-soluble derivatives of cellulose, with exceptional biocompatibility profiles and film-forming capacity (P.Sakellariou et al. 1995; Picart et al. 2014). Generally, HEC is obtained by the reaction of alkali cellulose with ethylene oxide (EO) (El Barkany et al. 2017), and it shows adequate solubility in water, when the molar ratio of EO to the anhydroglucose parts of cellulose is higher than 1.5. In addition, HEC is soluble in dimethyl sulfoxide and dimethylformamide. With its desirable biocompatibility, non-immunogenicity, and low toxicity, HEC can be a potential candidate for biomedical applications such as wound dressings and wound healing.

In the context of green chemistry and the call for the use of eco-friendly solvents, ILs have emerged as potential environmentally benign alternatives to conventional organic solvents. The low solubility of cellulose in water and organic solvents limits its modification (Ge et al. 2022). For this reason, new more efficient and ecological synthesis processes have been innovated (Mezzetta et al. 2019). These synthesis methods are based on the use of ionic liquids to dissolve and modify oligosaccharides such as cellulose. ILs can also be used in the development and elaboration of new materials and biomaterials for various industrial applications. A great effort has been made to develop Polyionic liquids (PILs) and to improve their physico-chemical properties. PILs based on cellulose and its derivatives have received enormous attention due to their interesting properties. However, quaternary derivatives of cellulose may be better candidates and more attractive for use because of their biocompatibility, biodegradability and low immunogenicity (Samal et al. 2012). Protonated chitosan is among the most used cationic polysaccharides in this field because of its ability to increase the permeation of peptide drugs through mucosal epithelia (Thanou et al. 2001). Given its solubility and charge limitations at neutral pH, many researchers have aimed to elaborate more effective chitosan derivatives as well as cationic derivatives of other polysaccharides such as cellulose. The idea is to alkylate the amine groups of chitosan in order to prepare quaternized ammonium derivatives with a permanent positive charge, which results in a greater solubility in the aqueous medium, appearing in a wide range of pH (Liu et al. 2016). Furthermore, in order to study the impact of surface properties on the ocular bioavailability of 5-fluorouracil (5-FU) Fabiano et al prepared nanoparticles based on chitosan. The presence of permanent positive charges in these materials increased the contact of the nanoparticles with the ocular surface, while the negative charges slowed the release of 5-FU (Fabiano et al. 2019).

Recently, further studies have been done to develop the appropriate synthetic conditions for ammonium and phosphonium derivatives of cellulose (Marks et al. 2016). This synthetic method is done in a regioselective manner by C-6 halogen displacement while maximizing the DS of the cationic substituent (Marks et al. 2016). In contrast, limitations in the degree of substitution and solubility, which resulted from repulsions between the positive charges accumulated in the increasingly cationic product, were observed (Liu et al. 2016). So as to overcome these limitations, a new strategy for a useful and efficient synthesis of cationic cellulose ester salts was developed (Liu et al. 2016). This process is based on replacing the trialkyl amine nucleophilic group with aromatic amines to increase the efficiency of bromide nucleophilic displacement reactions by these amines due to the greater nucleophilicity of these aromatic amines as well as their greater ability to disperse the positive charges. This synthetic method allows the preparation of cationic polysaccharides with the necessary properties, particularly charge density, for the desired biomedical applications. According to Liu (Liu et al. 2016), high DS values were observed for the cationic substituents and the obtained materials show better physicochemical properties, such as thermal stability, water solubility and permanent positive charge. In addition, these cationic derivatives of cellulose bind strongly to a hydrophilic and anionic surface (Liu et al. 2016). However, all these synthesized cationic cellulose ionomers were derived from microcrystalline cellulose (MCC) with a low degree of polymerization (DP). This low starting DP limits the usefulness of its derivatives for plastics and other applications where a high DP is required. Due to the limited availability of cellulose esters in the market, other processes for the elaboration of cellulosic PILs have been done. Liu, S., & Edgar et al have developed novel cellulosic PILs from commercial cellulose esters with high DP to overcome the of low DP of MCC. Furthermore, they found that the modification processes can be achieved with full chemoselectivity and regioselectivity (Liu et al. 2017).

Cellulosic PILs have a wide variety of industrial applications. They can be used as thickeners for mineral processing, and as conditioners in hair care products. By virtue of its permanent positive charge, Cellulosic PILs exhibit significant antibacterial properties while disrupting the bacterial membrane, which subsequently leads to cell death (Joubert et al. 2015). Recently, cellulosic PILs are also used in the purification of biofuels by a membrane process (Hassan et al. 2016), and as sorbents for CO_2 capture in order to achieve environmental protection using natural resources (L.Bernard et al. 2018). Thanks to their ability to flocculate dispersed systems with negatively charged surfaces, cellulosic PILs are widely used in this field of application.

Despite the wide range of uses of cellulose PILs in various fields and especially in the biomedical one, the surface of the polymer film that is in contact with water is still not known. Holly and Refejo have shown that even hydrogels have high water contact angles due to the overlaying of the surface with non-polar hydrophobic groups (Holly et al. 1975). They have also shown that the high hysteresis of the contact angle is due to the reorganization of the surface in contact with water.

Moreover, it is known that glassy amphiphilic homopolymers with low T_g show a rapid decrease of the contact angle because of the dynamics and the rapid reorganization of the surface in contact with water (Dhopatkar et al. 2018).

The Non-Covalent Interaction (NCI) plays a major role in many physical (Du et al. 2021; Li et al. 2021), biological (McClements. 2006; Guo et al. 2021; Watanabe et al. 2021) and chemical phenomena (T.Mahmudov et al. 2017; Banaru et al. 2021; J.Grabowski. 2021; Xu et al. 2021). The primary structure of polymers is governed by the covalent bonds between the various atoms and chemical entities, while their spatial structure is governed by various non-covalent, inter- and intra-molecular interactions. Currently, many theoretical studies are being conducted to describe, measure and understand the effects of non-covalent interactions on their systems (Atmani et al. 2021; Fang et al. 2021). Density functional theory (DFT) is one of the most widely used methods in quantum calculations of the electronic structure of matter, and it is also a popular and versatile method for producing realistic geometries and relative energies. In this context, the aim of theoretical calculation is to investigate the geometries in terms of inter and intra-molecular interaction and their effects on the agglomeration of positively charged systems.

Despite the significant interest in cellulose-based PILs, there is still a lack of studies on HEC PILs, which is the most important water-soluble derivative of cellulose. Also, in recent studies researchers have not achieved a high DS (DS_{max}= 0.74). To the best of our knowledge, no glassy and amphiphilic ester based on HEC and ILs with low

T_g are reported in literature. In this context, our work is based on the synthesis, characterization and determination of the physico-chemical properties of HEC-ILs.

The synthesis procedure used in this work involves only two steps. The first one aims to graft hydrophobic ester groups onto the HEC matrix using bromo acetyl bromide. The high reactivity of the acetyl bromide provides a high DS of ester group and alkyl bromide. The second step concerns the grafting of ionic liquids onto the HEC matrix in order to reveal the amphiphilic character in each repetitive unit of HEC.

Therefore, this work aims to elaborate new glassy amphiphilic materials based on HEC and to understand their behavior in contact with water. These materials are intended to be applied in various fields such as the biomedical and drug delivery (Liu et al. 2016; Milcovich et al. 2016; Shafiei-Irannejad et al. 2019; Vasiliu et al. 2019).

Experimental:

Materials:

HEC was obtained from the chemical modification of cellulose extracted from the esparto plant from the eastern region of Morocco according to the procedure described previously in (El Idrissi et al. 2013). Dimethylformamide (DMF) was obtained from the Fluka Company. Vinyl pyridine (VP), vinyl imidazole (VI) and methyl imidazole (MI) were obtained from Sigma Aldrich, and were used without any further purification.

Methods:

Instrumental analysis:

The chemical structures of the HEC, and HEC-IL samples were evaluated using FTIR technique. The spectra were recorded on JASCO FT/IR-4700 spectrometer using ATR attachment. An average of 70 scans were taken for each sample and recorded from 4000 to 350 cm^{-1}.

^{1}H NMR was used to characterize the synthesized HEC-ILs. Deuterated Dimethyl sulfoxide (DMSO) and deuterium oxide (D_2O) were chosen as a solvent and TMS as a reference. The spectra were recorded on a JEOL JNM-ECZ500R/S1 spectrometer. The elemental analysis of C, H, N, O have been performed using the EuroEA Elemental Analyzer.

DSC measurements were conducted using a DSC 204 F1 (Netzsch, Selb, Germany). The analysis was performed under a nitrogen atmosphere, with samples of approximately 4-5 mg at a scan rate of 10 °C/min from -70 to 500 °C. TGA was performed with a linear temperature increase (TGA-DTA, STA 449 C/4/MFC/G/Jupiter®, NETZSCH-Gerätebau GmbH, Selb, Germany). Thermogravimetric analysis was performed under a helium atmosphere of 40 mL/min at a constant flow rate. approx. 10 mg of the sample was heated from 25 °C to 600 °C at a rate of 10 °C/min.

XRD patterns of the samples were obtained with an Advanced D8 powder diffractometer (Brucker D8, Germany) using a Cu Kα (λ=1.5418 Å) radiation at 40 kV and 40 mA with a scan range of 4-2θ–80°, a scan speed of 0.02°2θ per 2 s, and a step size of 0.02° 2θ.

The ORIGIN software was used to calculate the crystallinity rate of different samples. the amorphous halo peak and the crystalline peaks are deconvoluted by origin software using the Gaussian function, and all peaks were ensured to fit the original spectrum. The crystallinity was calculated using the following equation:

$$\chi_c \,\% = \frac{A_c}{A_c + A_a} \qquad (1)$$

Ac: area under the crystalline peak.

Aa: area under the amorphous peak.

The surface morphology of the different samples was characterized using an SEM, Hitachi S-4800 (Accelerating voltage of 10 kV).

Anton Paar Litesizer was used to measure the zeta potential of the different samples. 3 separate essays were carried out for each sample. The dispersion of the HEC-ILs in different solvents was monitored by transmittance using the same apparatus (Anton Paar Litesizer).

The surface wettability of the HEC, HEC-Br, HEC-IL films was monitored by the contact angle. The contact angle of the different samples was measured using the KSV CAM 10 goniometer. This instrument measures the contact angle between 1° and 180° with an accuracy of ±1°.

Synthesis of HEC-Br:

1g of HEC was dissolved in DMF, and 0.0262 moles of bromo acetyl bromide (2eq/OH) was added to the mixture. The mixture was stirred at a temperature of 60°C for 5 hours. The product was isolated by precipitating the mixture in an excess of distilled water, filtered and dried under vacuum to a constant weight.

Synthesis of HEC-ILs:

1g of HEC-Br was dissolved in THF, and 2eq/Br of vinyl imidazole was added. The mixture was stirred at a temperature of 60°C. After 40 min of reaction, a precipitate appeared. The reaction was stirred for 72 h and the product obtained was isolated by filtration. Then, it was washed and dried under vacuum to a constant weight.

For vinyl pyridine and methyl imidazole, the same approach was followed to modify the HEC-Br.

Dispersion of HEC-ILs in organic solvents:

The HEC-IL samples were freeze-dried using the Christ Alpha 2–4 freeze-dryer to remove traces of water and organic solvents. 5 mg of each sample was then dispersed in 5 ml of solvent (1wt%) and sonicated to obtain a stable suspension. A variety of solvents were chosen (methanol (MeOH), acetonitrile (ACN), tetrahydrofuran (THF), acetone). The dispersion of HEC-ILs in the different organic solvents was monitored by transmittance as a function of time (0 h-24 h).

Computational details:

The geometries of a single monomer of modified cellulose (HEC-MI) have been optimized using DFT at the level of a B3LYP/**6-31G** calculation using the Gaussian 9 program (Frisch et al. 2009). Materials Studio Software is used to study the polymer structure (based on the optimized monomer), The DFT results were obtained using the DMol3 (Bernard. 1990, 2000) and the GGA functionals were PW91 (Perdew et al. 1992) in conjunction with the double numerical basis set DNP. The NCI and molecular electrostatic potential (MESP) were calculated using the Multiwfn program (Lu et al. 2012). The mapped iso-surface was obtained by VMD 1.9.2 program (Humphrey et al. 1996).

Results and discussion:

In this work, we grafted ILs onto HEC matrix (Fig. 1). The synthesis was carried out in two steps. The first step is the modification of HEC with bromo acetyl bromide in DMF to form HEC-Br. The second step involves the nucleophilic substitution of HEC-Br with vinyl pyridine, vinyl imidazole, and 1-methyl imidazole. HEC-Br is soluble in THF. Once the cyclic amines are quaternized the solution becomes cloudy. The partial solubility of the polymer in THF can be explained by the lack of hydrophobic chains and the appearance of electrostatic and hydrophobic-hydrophilic interactions, which are stronger than the hydrophobic-hydrophobic ones. As the reaction time increases, the degree of quaternization increases, resulting in the formation of microdomains and a microscopic precipitate appearing in the reaction medium. A phase separation was observed at this stage due to intermolecular interactions, which are predominant over polymer-solvent interactions. The selection of cyclic amines is due to their high nucleophilic character compared to aliphatic amines. The aromatic substituent allows us to disperse the positive charge well. Consequently, these two properties of cyclic amines allow us to improve the DS and the quaternization degree.

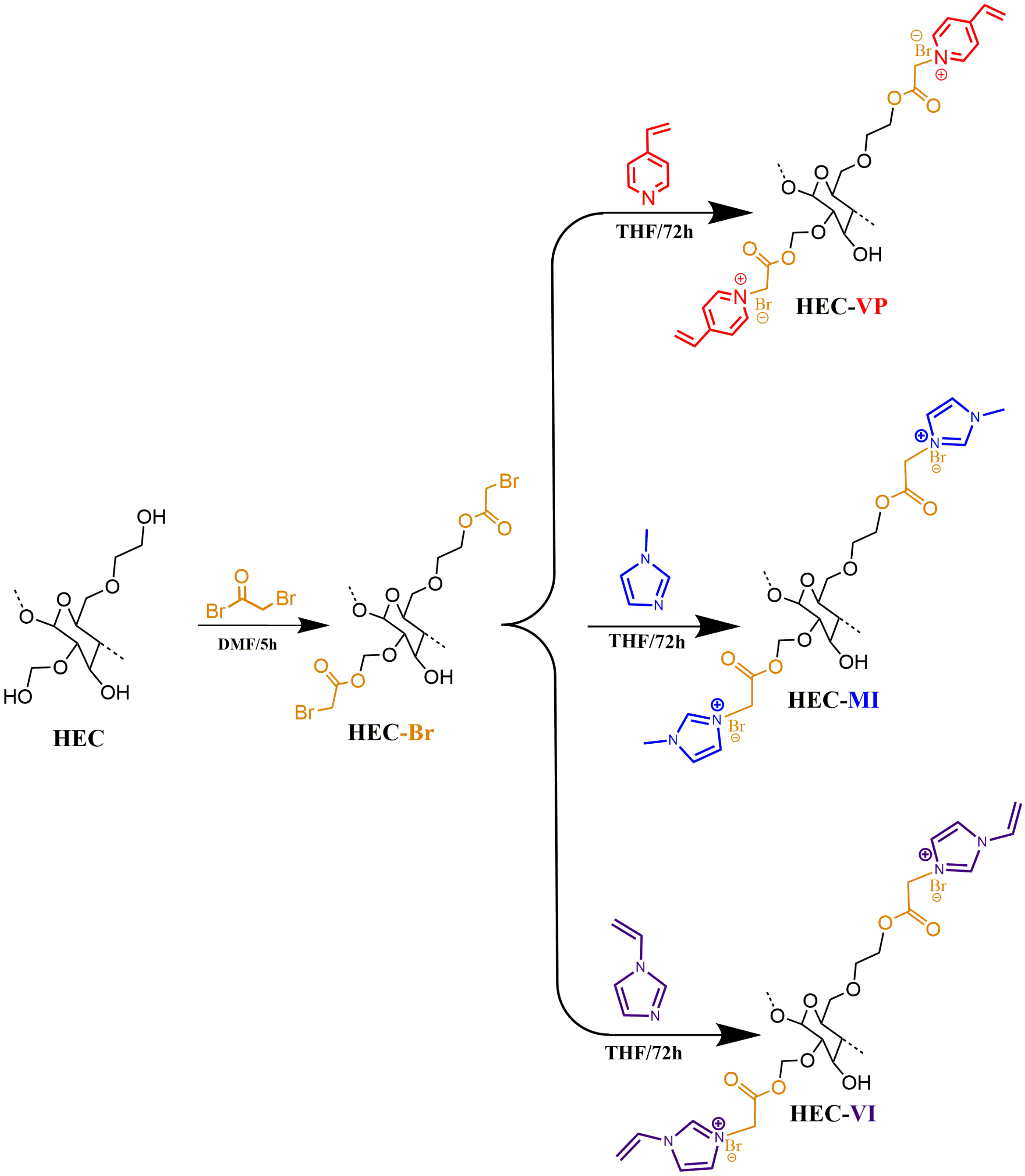

Fig.1 Reaction scheme for the preparation of HEC-ILs from HEC

FTIR-ATR Analysis:

The modification and the grafting of ILs onto HEC matrix was followed by FTIR. The appearance of new characteristic absorption bands on one side and the disappearance of others allows us to verify the success of the incorporation reaction of ILs in the HEC matrix.

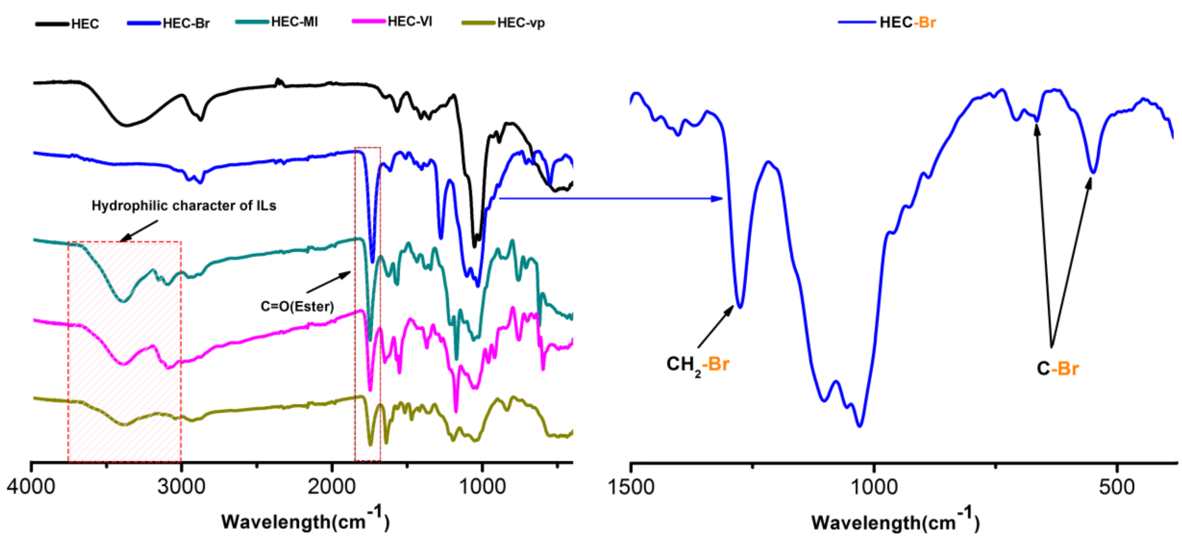

Fig.2 FTIR spectrum of HEC, HEC-Br and HEC-ILs

The FTIR spectrum of HEC-Br shows the successful grafting of bromo acetyl bromide onto the HEC matrix (see details in the supplementary information). In the infrared spectrum of HEC-g-vinyl imidazolium bromide (HEC-VI) (Fig.2), new absorption bands appeared, corresponding to the scratching of VI-IL on the HEC matrix. The bands at 3140, 1650, and 1624 cm^{-1} are attributed to the C-H, C=C and C=N of the vinyl imidazolium group, respectively (Chen et al. 2012). Another sign of vinyl imidazolium group insertion success on the HEC matrix is the appearance of new characteristic bands around 3098, 995 and 985 cm^{-1} which corresponds to the vibration mode of elongation and out-of-plane deformation of =C-H (Chen et al. 2012). The FTIR band observed at 747 cm^{-1} is attributed to the stretching vibration of the C-N bond that connects the imidazole cycle to the vinyl part (MuzafferTalu et al. 2015). The characteristic band at 664 cm^{-1} was attributed to the folding vibration of the imidazole cycle (MuzafferTalu et al. 2015). The bands centered around 1576, 1552 and 1218cm^{-1} are attributed to the -C-C-, -C-N- and the bending of the C-H chain with C=N stretching of the imidazole (MuzafferTalu et al. 2015). In contrast, the disappearance of the characteristic bands of the CH_2-Br and C-Br bond indicates the success of the modification of HEC by vinyl imidazole (Suna et al. 2009; Liu et al. 2016).

The addition of 1-methyl imidazole to HEC-Br shows new absorption bands, which appear around 1177,1568 and 1635 cm^{-1} corresponding respectively to the vibrations of the C-N, C=C and C=N bonds of methyl imidazole (Chen et al. 2012). Moreover, the bands that appear around 3102 3163 cm^{-1} are attributed to the C-H stretching vibration mode of the imidazole ring (Chen et al. 2012). The increase in the intensity of the band located around 3395 $cm\text{-}^{1}$ is due to the hydrophilicity of the imidazolium moiety. The disappearance of the bands around 1276, 647 and 547 cm^{-1}, which characterizes the CH_2-Br and C-Br bonds respectively (Suna et al. 2009; Liu et al. 2016), indicates the fixation of imidazolium on the HEC-Br chains.

Similarly, for HEC-g-vinyl pyridinium bromide (HEC-VP) spectrum (Fig.2), the bands that appear around 3137, 1603 and 1193 cm^{-1} are attributed respectively to the C-H, C=C and C-N of the pyridine group (Chauhan et al. 2004; Li et al. 2014a; Xue et al. 2015). The characteristic bands of the vinyl group are centered at about 3042, 1644 and 883 cm^{-1} which corresponds to the elongation of the =C-H bond (L.Bernard et al. 2018), C=C and the out-of-plane deformation of =C-H. Due to the quaternization of the pyridine group and the formation of pyridinium, the vibration characteristic band of the C=N bond is overlapped with the characteristic band of the vinyl C=C bond at about 1644 cm^{-1}.

^{1}H, ^{13}C NMR Analysis:

This section deals with the characterisation of the products obtained using the NMR technique. The Spectral analysis of HEC-Br ^{1}H NMR and ^{13}C NMR spectrum reveals new signals (interpreted in supplementary information).

The structural analysis of the HEC-VI compounds using ^{1}H NMR shows in its spectrum the formation of the desired structure by the presence of a signal at 9.1 ppm corresponding to the quaternary proton of the imidazolium ring (Fig. 3.b). The methylene (O=C-**CH_2**-N^+-) between the carbonyl and ammonium groups appears around 5 ppm. We noted the appearance of two multiples around 5.33-5,76 ppm corresponding to the protons of the vinyl group of vinyl imidazole. Moreover, a quadruplet situated around 7.08 ppm corresponds to the vinyl proton on α of the imidazolium group nitrogen. The signals of the methylene protons on α of the various hydroxyl groups are located at ~ 3.6 ppm, and those attached to the carbon (C6) of the cellulosic skeleton give signals at around ~ 3.5 ppm (El Idrissi et al. 2013). The signal that appeared at 4.15 ppm corresponds to protons of methylene (-**CH_2**-O-C=O) on α of the ester. The ^{13}C NMR spectrum (Fig. 3.e) also confirmed the identification of HEC-VI; the new resonances at 110-138 ppm are attributed to the carbons of the added vinyl imidazolium substituent. In addition, the disappearance of the **C**-Br peak at 37 ppm, and the appearance of a new peak at 52 ppm characteristic of the carbon linked to the imidazolium group (O=C-**C**H_2-N^+-) confirms the success of the reaction (Liu et al. 2017).

Similarly, the analysis of the ^{1}H NMR spectrum of HEC-g-methyl imidazolium bromide (HEC-MI) (Fig. 3.a) shows the success of the quaternization reaction of the imidazole group by HEC-Br. The first indication is the appearance of the quaternary proton of the imidazolium group around 9.12 ppm. The second is the appearance of a peak around 7.67 ppm corresponding to the other two protons of the imidazolium ring. In addition, a peak was observed at 3.83 ppm corresponding to the methyl group (N-**CH_3**) of the imidazolium methyl (Liu et al. 2017). Moreover, the methylene group on α of the quaternary nitrogen shows a signal around 4.91 ppm. The characteristic peaks of the HEC-Br backbone appeared around 3.45, 3.6 and 4.2 ppm (El Idrissi et al. 2013). The ^{13}C NMR spectrum of HEC-MI (Fig. 3.d) shows the appearance of new peaks around 123-137 and 36.15 ppm characteristic of the imidazole ring. Another peak appeared around 51.26 ppm characteristic of the carbon linked to the imidazolium group (O=C-**C**H_2-N^+-) which confirms the quaternisation of the imidazole group by HEC-Br (Liu et al. 2017).

In the same context, the spectral analysis of HEC-VP (Fig. 3.c) shows the grafting of vinyl pyridinium onto the HEC matrix. The vinyl group shows signals in the range of 5.46-6.99 ppm. The quaternization of the pyridine nitrogen shows a signal around 8.7 ppm corresponding to the protons on α of the quaternary nitrogen. The other protons of the pyridinium ring appear around 8.13 ppm (Liu et al. 2017). Because of the mesomeric effect of the pyridine ring, the peak corresponding to the (O=C**-CH_2**-N^+-) group directly linked to the quaternary nitrogen has been shifted to 5.3 ppm. The ^{13}C NMR spectrum (Fig. 3.f) shows new signals around 120-149 ppm and 60 ppm characteristic of the vinyl pyridinium group and the carbon attached to it (O=C-**C**H_2-N^+-) respectively (Liu et al. 2017).

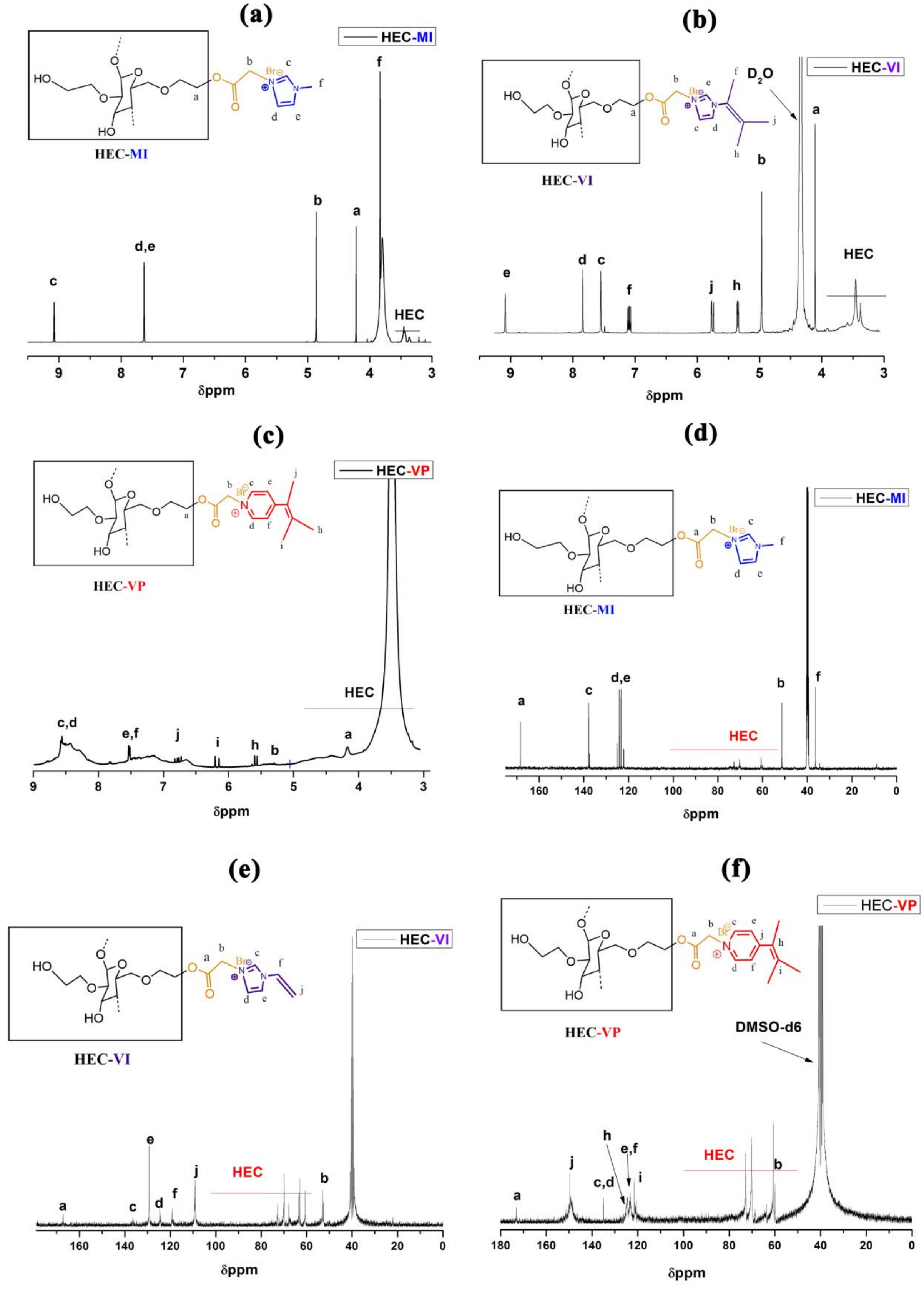

Fig.3 ^{1}H NMR spectrum of HEC-MI (a), HEC-VI (b), HEC-VP (c); ^{13}C NMR spectrum of HEC-MI (d), HEC-VI (e), HEC-VP (f)

It was also noted that the results of ^{1}H NMR and ^{13}C NMR analysis of HEC-Br, HEC-MI, HEC-VI and HEC-VP agree with the proposed structures and with what is available in the literature.

Elemental analysis:

The elemental composition of the products was determined with the EuroEA elemental analyzer from powder samples. CHNO of HEC, HEC-Br, HEC-ILs were used to prove the grafting of ILs on HEC. The mass percentages of hydrogen, carbon, oxygen and nitrogen were measured, and the results are reported in Table 1. The CHNO results show the appearance of nitrogen in the HEC-IL samples, which indicates that the grafting of HEC by ILs was successfully affected. The DS and degree of quaternization (DQ) were then calculated by formula (Şen et al. 2018) (2) and (3):

$$DS = M_{AGU} * \frac{\frac{X_N}{n}}{(100*M_N)-\left(M_{g.g}*\frac{X_N}{n}\right)} \qquad (2)$$

$$DQ = \frac{DS_{(HEC-ILs)}}{DS_{(HEC-Br)}} * 100 \qquad (3)$$

Where:

X_N is the molar fraction of nitrogen. M_{AGU}: the molecular weight of anhydroglucose unit.

M_N is the atomic weight of nitrogen. $M_{g.g}$: the molecular weight of grafted group.

n: number of nitrogen atoms in the grafted group.

DS (HEC-ILs) is degree of substitution of HEC-ILs.

DS (HEC-Br) is degree of substitution of HEC-Br.

Table 1 CHNO elemental analyses of HEC, HEC-Br, HEC-ILs, DS, and DQ using EA

Element	N %	C %	H %	O %	DS (EA)	DQ %(EA)
HEC	0	52.151	8.390	39.459	-	-
HEC-Br	0	32.081	3.860	29.408	2.46	-
HEC-MI	7.301	35.918	4.295	22.712	1.424	57.89
HEC-VI	7.968	37.306	4.369	20.492	2.325	94.51
HEC-VP	3.720	42.067	5.035	19.575	2.329	94.67

The results of the DS calculations show high values compared to those found by Hassan et al who grafted ionic liquids onto cellulose acetate and achieved a DS_{max} of 0.5 (Hassan et al. 2016). The advantage of these materials over those found in the literature is that we have been able to enhance the DS, while applying a synthesis strategy that allows us to increase the DS of the ester and bromine groups in the extrimity of the chain. This increase in DS will then give us the desired surface and thermal properties (such properties especially the T_g decrease and reorganisation of the surface in contact with water will be discussed more thoroughly in the DSC Analysis and Contact Angle measurement sections).

Thermogravimetric Analysis :

The grafting of ILs on HEC main chain influences the thermal stability of these materials. This influence was investigated by thermogravimetric analysis. The thermograms show that the thermal stability of HEC was slightly higher than that of the prepared derivatives.

The thermogravimetric curves of the unmodified HEC and modified HEC samples (HEC-VP, HEC-VI and HEC-MI) are shown in Fig.4.a. The thermal stability of HEC and HEC-Br has been investigated in detail (supplementary information). Concerning HEC-ILs, the degradation occurs in two stages: the first mass loss, situated between room temperature and 100 °C, was attributed to the loss of water physically absorbed at the surface and remaining solvents. The second mass loss occurred in the temperature range of 210 °C and 350 °C with a mass loss of 66 %, 67 % and 57.3 % for HEC-MI, HEC-VI and HEC-VP respectively, which was attributed to the elimination of imidazolium or pyridinium group (L.Bernard et al. 2018), and the decomposition of HEC main chains (El Idrissi et al. 2013; Chen et al. 2015). The loss of mass at temperatures above 400°C is attributed to the carbonization of the degraded products(Fei et al. 2018). It can be concluded that the decrease in the degradation temperature of HEC- ILs may be due to the decrease in their crystallinity (El Idrissi et al. 2013).

Differential Scanning Calorimeter :

DSC was used to assess the influence of the HEC modification by ILs on the thermal properties, especially on the T_g. As mentioned in the studies of Freitas et al, which have investigated the impact of DS on the thermal properties of cellulose acetate (CA), increasing the DS of the ester group leads to a decrease in T_g (Freitas et al. 2017). Furthermore, Hassan et al. remarked that the modification of CA by ILs induces a strong decrease in T_g and the plasticizing effect of ILs increases with the mobility of ILs (Hassan et al. 2016). However, they were unable to achieve negative T_g values which may be due to the small ($DS(ILs)_{max}$=0.5) DS values. Hence, we thought of grafting bromo acetyl bromide and ILs onto HEC to achieve T_g <0°C values while increasing both the DS of the ester and the ILs.

The glass transition temperatures (T_g) of HEC, HEC-VI, HEC-MI and HEC-VP appear around 139°, -49, -48 and -38°C, respectively (Fig.4.(b.d.f.g)). The T_g of HEC grafted with ILs increases with the melting temperature (Tm) of related molecular ILs (Fig.4.b) (Hassan et al. 2016). The difference between the T_g of HEC and HEC-ILs can be explained by the grafting of ester groups and ILs onto the HEC matrix. The acetyl groups decrease the intensity of hydrogen bond formation, and lower temperatures are required for the onset of the T_g event. From the T_g values of these prepared polymers, we succeeded in decreasing the T_g by grafting esters and ILs onto HEC with a high DS. This decrease in T_g gives us desirable properties such as flexibility and better surface dynamics which allows it to reorganize rapidly in contact with water.

The DSC curves of HEC and HEC-ILs (Fig.4.(b.d.f.g)) show an endothermic event visible for all samples corresponding to the vaporization of adsorbed water. This event is observed at around 77°C. In general, polysaccharide-based PILs are known to adsorb moisture. As a result, desorption occurs, and a broad peak appears in the DSC curve. The variation of the values of this peak from one product to another can be explained by the different water retention capacities and polymer-water interaction. This is due to the tendency of the hydroxyl and amine groups of the polymer to form hydrogen bonds with water.

HEC-MI shows a typical crystal structure with a melting peak at 103°C from the first heating cycle (Fig.4.g). Furthermore, the crystallization temperature (T_c) appeared at 2°C. The melting temperatures of HEC-VI and HEC-VP are very close to each other in an order of 257 and 267°C, respectively.

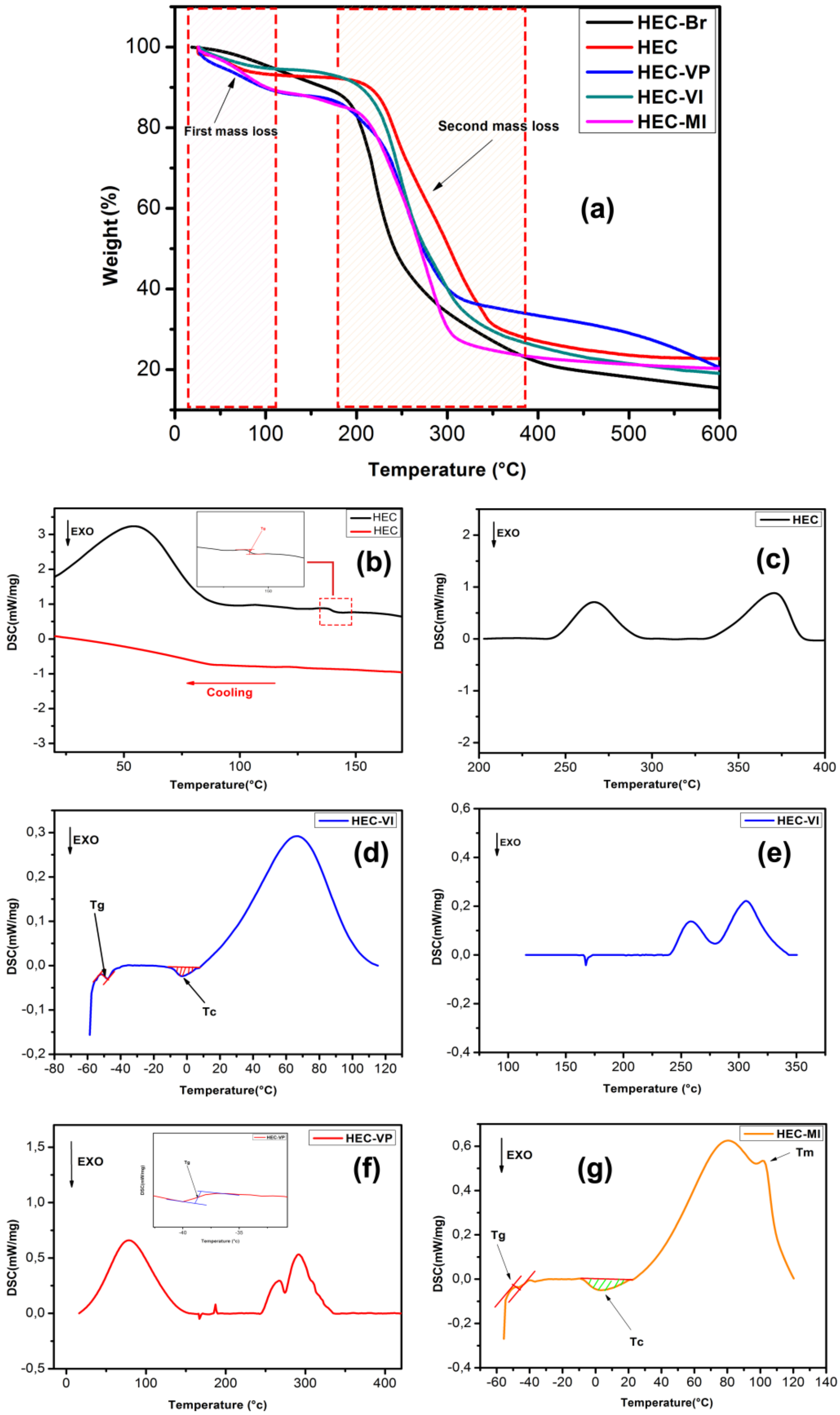

Fig.4 TGA profile of HEC, HEC-Br, HEC-MI, HEC-VP and HEC-VI (a); DSC curves of HEC (b,c); HEC-VI (d,e); HEC-VP (f); HEC-MI (g)

X-ray diffraction :

Changes in the structure can be evaluated by X-ray diffraction. The diffractograms of HEC and HEC-ILs are shown in Fig.5.a. The diffractogram of HEC confirms the semi-crystalline structure of this polymer (Trivedi et al. 2015). XRD patterns of HEC show 3 characteristic peaks appearing at 2θ=8.39°,20.75° and 38.4°, corresponding to the ($\bar{1}10$), (020) and (004) planes, respectively (D.French. 2014). The crystallinity can be evaluated by the Hodge method, which established a correlation between the intensity, the width of the peak and the crystallinity (R.M.Hodge et al. 1996). The modification of HEC by ILs produced remarkable changes in the crystal structure of HEC. Similar changes were observed for all HEC-IL samples: the peak located at 20.75° becomes broad and shifts to high 2θ values with a decrease in peak intensity. Furthermore, the quaternization of the imidazolium and pyridinium amines resulting in the appearance of new characteristic peaks at 2θ= 13.21°, 28° and 62°, confirming the attachment of ILs to HEC. From the XRD patterns of HEC-ILs, it can be observed that the crystallinity decreases following this order HEC>HEC-MI>HEC-VI>HEC-VP.

To investigate the amorphous nature of our polymers in a more precise way, the deconvolution technique was chosen (Wang et al. 2015; N.Hafiza et al. 2017). The deconvolved diffractograms are presented in Fig.5.(b.c.d.e). The crystalline peaks are shown in green dotted lines and the amorphous peaks are shown in red lines.

Table 2 Crystallinity of HEC, HEC-MI, HEC-VI and HEC-VP

Samples	A_c	A_a+A_c	χ_c %
HEC	26.57	132.18	20.10
HEC-MI	20.68	115.21	17.94
HEC-VI	12.82	93.40	13.73
HEC-VP	11.73	117.68	9.96

The crystallinity values are presented in table 2. The results confirm the decreasing crystallinity sense found by the method of comparing intensities, widths and displacements of peaks described in the previous section. HEC shows a degree of crystallinity of 20.10%, which is similar to that found in the literature (Li et al. 2014b; Wang et al. 2015; N.Hafiza et al. 2017). HEC-MI, HEC-VI, HEC-VP have a crystallinity degree of 17.94, 13.73, 9.96%, respectively. From these results, it can be concluded that HEC-ILs have an amorphous structure; it is noted that only a slight decrease in crystallinity was noticed.

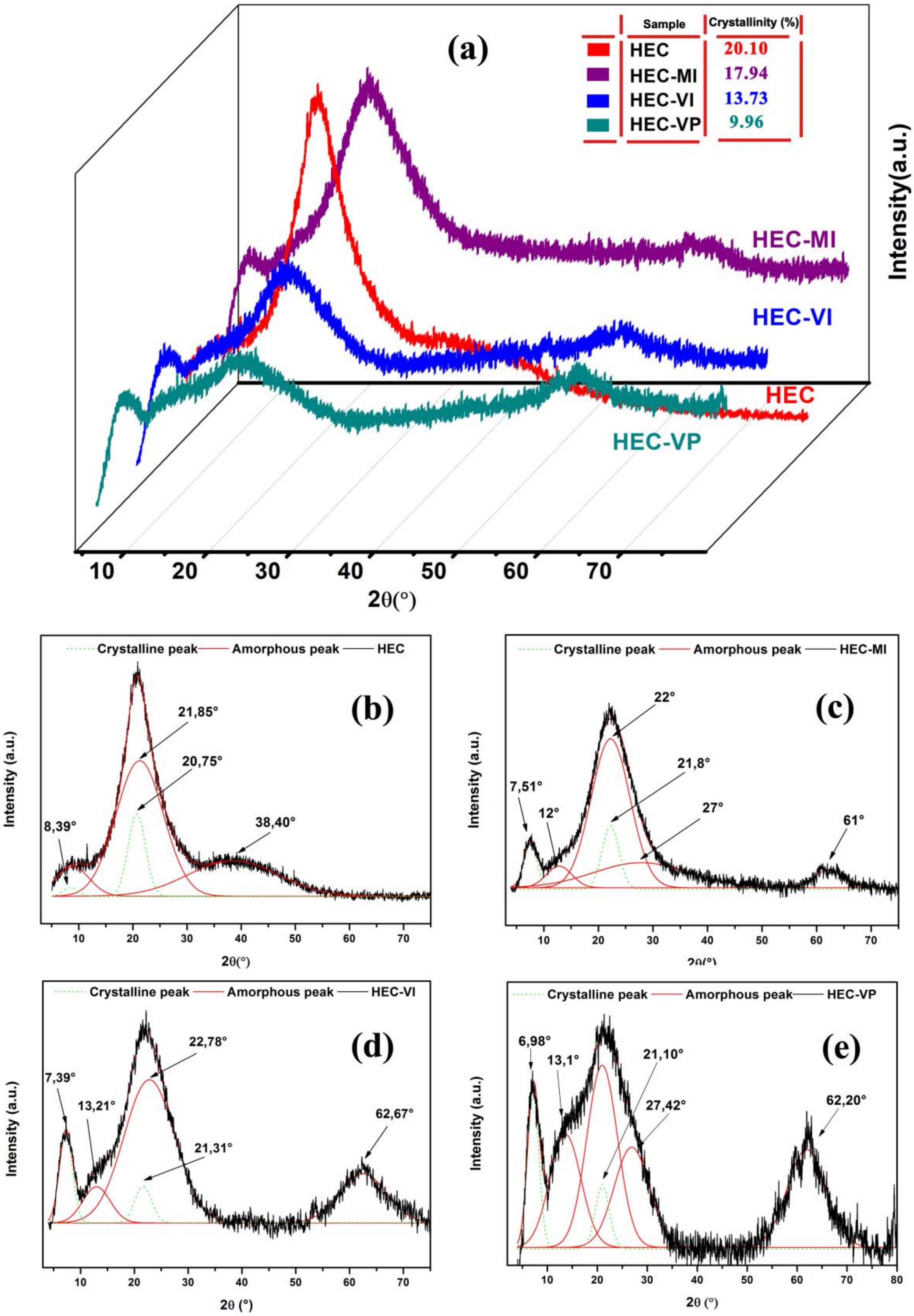

Fig.5 X-ray diffractogram of HEC, HEC-MI, HEC-VP and HEC-VI (a); deconvoluted XRD of HEC (b); HEC-MI (c); HEC-VI (d); HEC-VP (e)

Scanning electron microscopy :

Figure 6 shows SEM images of HEC (a), HEC-Br (b), HEC-VI (d), HEC-MI (c), and HEC-VP (e). The micrograph of HEC-Br (Fig.6.b) shows that after the modification of HEC, the morphology changes from the typical fibrous appearance to a compact appearance with a homogeneous and smooth surface. SEM images of HEC-VI (Fig.6.d) show that after the quaternization reaction and grafting of ionic liquids onto HEC, the morphology remains compact but with an agglomeration of HEC fibers with an oval and spherical shape and an average diameter of 6-10 µm (L.Bernard et al. 2018). This agglomeration may be originated from intra- and intermolecular interactions of the quaternized chains. The particle size is classified as small, as their average diameter is below 10 µm. HEC-MI and HEC-VP (Fig.6.(c.e)) show a similar surface morphology with a slight decrease in particle size compared to HEC-VI.

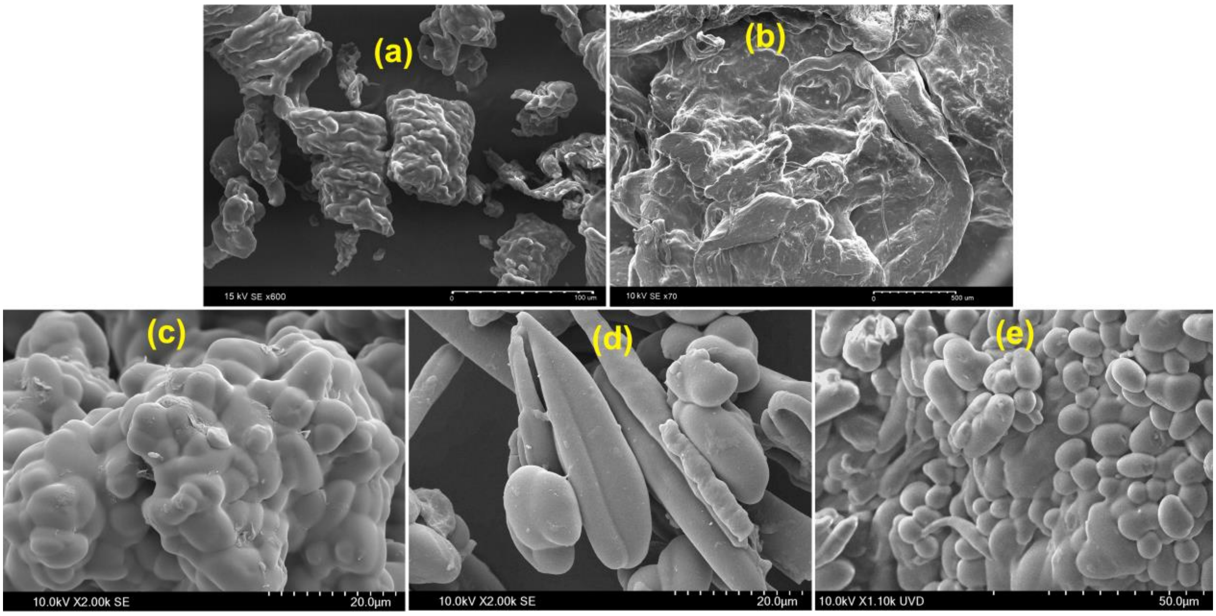

Fig.6 SEM images of HEC (a); HEC-Br (b); HEC-MI (c); HEC-VI (d); HEC-VP (e)

Water solubility and dispersion of HEC-ILs in organic solvents:

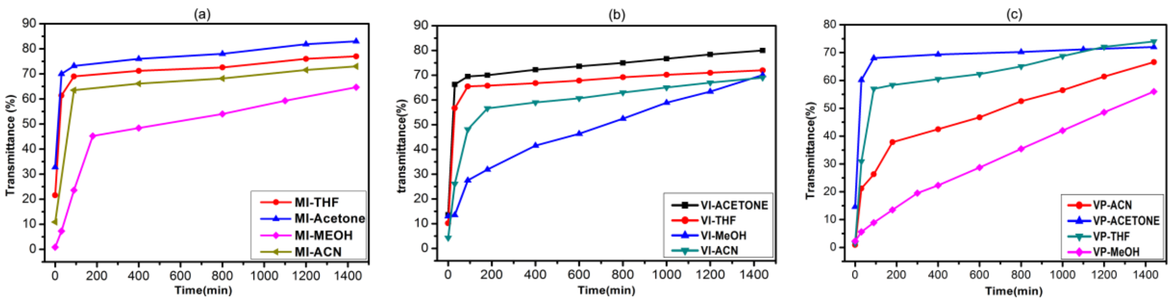

Fig.7 Dispersion of HEC-ILs in organic solvents

The successful preparation of amphiphilic polyelectrolytes based on HEC is not sufficient for their application in various fields, be it biomedical or coatings. The question is whether these cationic polyelectrolytes would have sufficient water solubility for these applications. Based on the solubility tests, it was found that these materials have good solubility in water. On the other hand, a zeta potential measurement was made to confirm the presence of positive charges and the preparation of the cationic polyelectrolytes. The zeta potential values of HEC-VP, HEC-MI, and HEC-VI are +30mV, +21mV, and +16 mV, respectively (Fig.8.b), which confirms the cationic aspect of these materials.

The dispersibility of the modified HECs in different solvents was tested. The stability of the suspensions was monitored by transmittance versus time. The stability of the suspensions depends on several parameters, such as electrostatic charge repulsion, affinity of the solvent with the material and also on the contact angle (Miao et al. 2016). Figure 7 shows the dispersibility results of HEC-ILs in a variety of organic solvents (MEOH, ACN, THF, ACETONE). The transmittance results show that the suspension of HEC-VP in MeOH is the most stable compared to the other organic solvents. Moreover, the stability of the colloidal systems decreases in the order MeOH>ACN>THF>ACETONE. The polarity of the solvents used may explain this decrease in the stability of the different suspensions. In addition, when comparing the stability of the suspensions of the different prepared materials, it is observed that the HEC-VP suspension is more stable than that of HEC-VI and HEC-MI. This phenomenon can be explained by the difference between these materials in zeta potential (+30mV for HEC-VP, +21mV for HEC-MI and +16mV for HEC-VI). Generally, it is known that when the zeta potential increases, the stability of the suspensions increases (Gu et al. 2020).

Contact angle:

The contact angles of the different materials are presented in fig.8.a. The variation of the contact angles of the thin films with time was used to follow the surface reorganization of HEC-ILs in contact with water and to confirm their amphiphilic character. The HEC film shows a contact angle of about 42,78°, which confirms its predominantly hydrophilic character (caused by the presence of polar hydroxyl groups on the HEC surface) compared to the hydrophobic one (resulting from the presence of lipophilic pyranose groups) (C.Malaspina et al. 2019). HEC-Br shows a hydrophobic character with a contact angle of 115,53°. This is resulted from the modification of the hydroxy groups of HEC by ester groups. The high contact angle of HEC-Br confirms the high DS of HEC-Br.

HEC-MI and HEC-VI show almost similar behavior. At the first contact of the water droplet with the surface of the thin film, the contact angle of HEC-MI and HEC-VI becomes 91,13° and 94,05°, respectively. In the course of time, a very fast decrease of the contact angle was observed until a scattered water droplet was obtained on the film surface. This sequence of contact angle evolution, which goes from hydrophobic to hydrophilic, confirms the amphiphilic behavior of our materials. Concerning HEC-VP, the same behavior was observed. The only difference that was noticed was the decrease in the speed of the contact angle. HEC-VP presents a contact angle of 101,75° at the beginning, but with time, it decreases at a relatively slow speed compared to HEC-MI and HEC-VI. This slow decrease of the contact angle speed can be explained by several parameters, among which we find the T_g, the interfacial energy, % of hydrophilic groups, and the ability to donor hydrogen bonds, etc.

Dhopatkar et al. have shown that as the T_g is lower, the surface becomes dynamic, hence the rapid decrease in contact angle (Dhopatkar et al. 2018). HEC-VP has a T_g of -38°C, which is relatively high compared to HEC-MI and HEC-VI (-49°C). This difference in T_g may explain the slow decrease in contact angle of HEC-VP compared to HEC-MI and HEC-VI. Another possible factor is the ability to form hydrogen bonds. Generally, imidazolium groups have a higher hydrogen bond donor ability than pyridinium ones (Hassan et al. 2016). This explains the strong interactions between water molecules and imidazolium groups, resulting in a rapid decrease in the contact angle compared to the pyridinium group. From these contact angle results, it can be concluded that these amphiphilic glassy polyelectrolytes can reorganize rapidly in contact with water. These properties open up a wide range of applications, especially in the biomedical field.

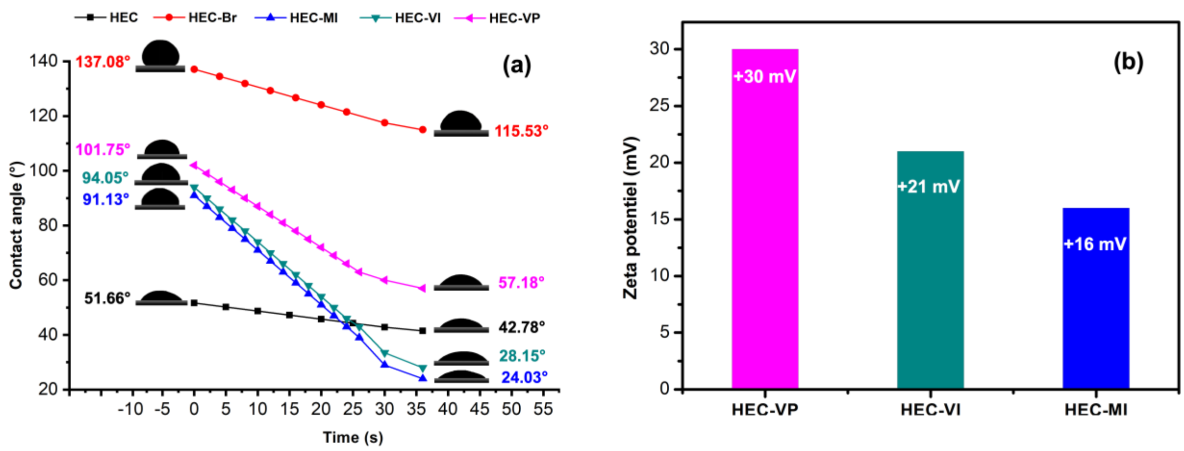

Fig.8 contact angle of HEC, HEC-Br, HEC-MI, HEC-VI, HEC-VP (a); zeta potential of HEC-ILs (b)

NCI & MESP Analysis:

The NCI method focuses on areas of low density which represent weak or non-covalent interactions. This approach allows visualization and quantification of the strengths of such interactions. The NCI technique is based on the analysis and graphical interpretation of the electron density and its derivatives in terms of its reduced gradient **RDG(r)**:

$$\mathrm{RDG(r)} = \frac{1}{2(3\pi^2)^{\frac{1}{3}}} \frac{|\nabla \rho(\mathrm{r})|}{\rho(\mathrm{r})^{\frac{4}{3}}} \qquad (4)$$

The reduced density gradient (ρ) is a parameter used to describe the deviation from a homogeneous distribution of electrons.

The reduced gradient will have very large positive values for remote regions of the molecule where the density approaches zero. Conversely, the reduced gradient will assume very low values, close to zero, for regions of covalent bonding and non-covalent interactions. The NCI method is essentially based on the visualization of those places in space where the reduced gradient (ρ) is close to zero.

In order to distinguish between the type of the interactions, the density was based on the sign of λ_2, with an RGB coloring scheme to classify the interactions:

$$\Lambda(\mathrm{r}) = \mathrm{sign}(\lambda_2) * \rho(\mathrm{r}) \qquad (5)$$

A scatter-plot between Λ(r) and RDG is presented in fig.9-b.

The intra and intermolecular interactions were determined by the analysis of reduced density gradient (RDG) calculations based on the analysis of non-covalent interactions (NCI) existing in HEC-MI. These analyses were carried out with an iso surface value of 0.5 and are displayed in fig.9-a. The blue, green and red regions represent respectively the H-bond interactions, the VDW interactions and the steric effect.

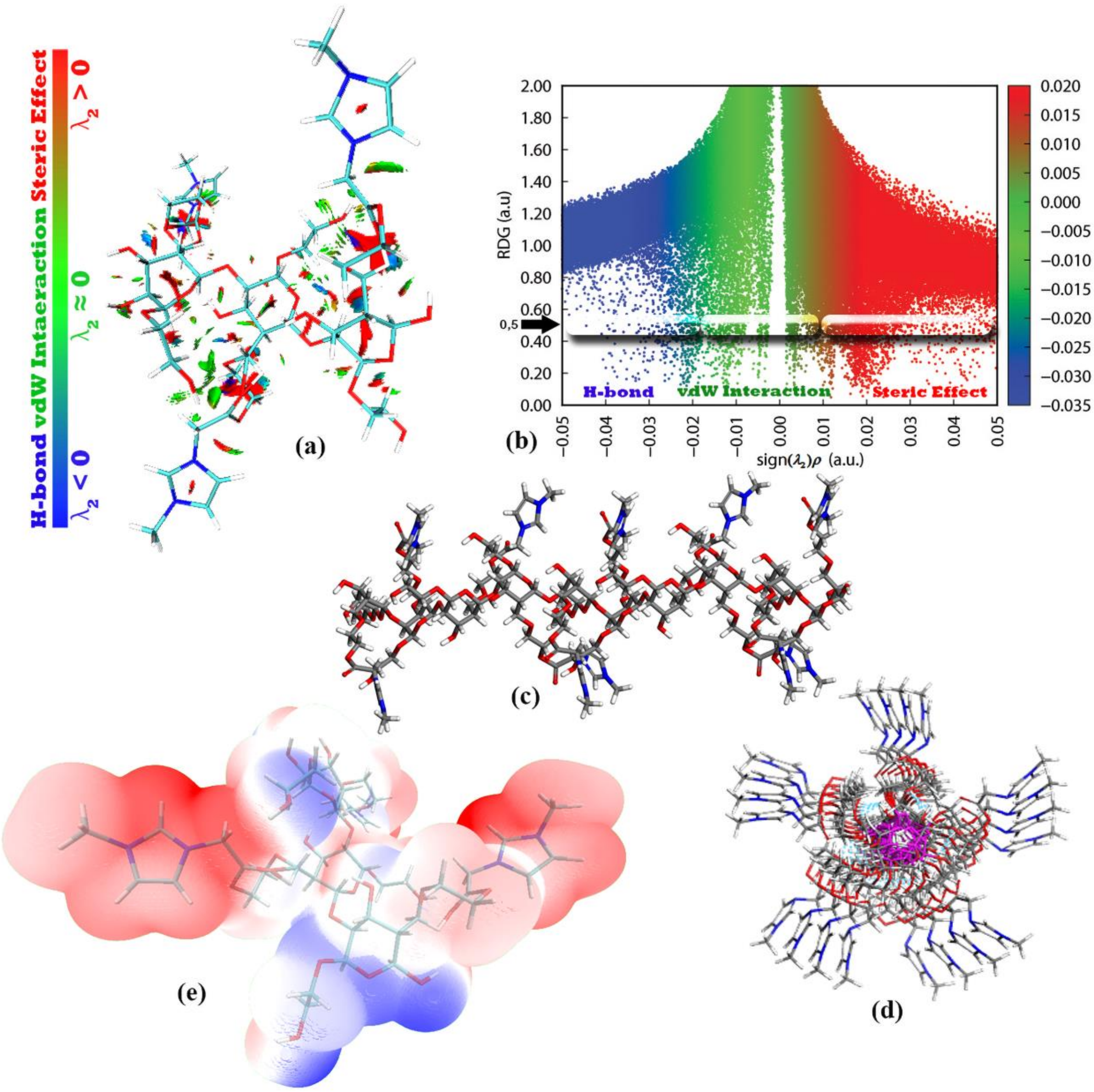

Fig.9 (a) RDG vs sign(λ_2)r for the HEC-MI (3 units) ; **(b)** RDG iso-surface for the HEC-MI. ; **(c) & (d)** Optimized structure of HEC-MI using Dmol3 -Top **&** side view ; **(e)** MESP Analysis

In the NCI-RDG isosurface plots (**Fig** 9-a & b), the blue region of hydrogen interactions is observed between the imidazolium group (pyridinium group for HEC-VP compound) and hydroxy group of HEC. The same interaction was noticed with the ether groups of the main chain of HEC. VDW- interactions (the green region) have also appeared throughout the same imidazolium group (pyridinium group for the compound HEC-VP). Red regions can be found in the center of the aromatic rings and near the HEC ether groups of the main chain showing the effect of steric repulsion. MESP is related to electron density, and it is a descriptor in the detection of electrophilic and nucleophilic attack sites and hydrogen bonding interactions. This descriptor illustrates the charge distributions of molecules in three dimensions to determine how molecules interact with each other, and it is also used to determine the nature of chemical bonds (fig.9-e). By analyzing MESP of HEC-MI, intermolecular interactions could be expected due to the spatial geometry of the chains, and π-π interactions can also be noticed. The intermolecular interaction energy minimization changes the position and orientation of the chains which causes a modification of the spatial arrangement (fig.9-c & d). Therefore, we can conclude that these compounds have a high agglomeration tendency.

Conclusion:

The modification of HEC with bromo acetyl bromide was done by a simple, fast, and efficient esterification reaction with a high DS. The obtained HEC-Br has good properties, namely solubility in a wide range of organic solvents and an attractive film-forming capacity. In addition, the HEC-Br film has a superhydrophobic and glassy character with a contact angle greater than 100° and a low T_g. The bromide existing at the end of the cellulose ester allows us to develop a simple and efficient process of HEC-IL elaboration.

The grafting of the esters and ILs onto the HEC matrix allowed us to obtain glassy (T_g less than 0°C) and amphiphilic bio-homopolymers with improved properties. The zeta potential confirms the success of the reaction and the presence of the expected permanent positive charge. The prepared HEC-ILs have good solubility in water. The study of the contact angle and the behaviors of HEC-ILs with water showed that the surface of these materials is capable of fast reorganization. The attractive properties of the developed HEC-ILs, namely water solubility, amphiphilic character, permanent positive charge and quick surface reorganization-ability open a wide range of applications in drug delivery and the biomedical field.

Acknowledgements:

A special thanks to the reviewers for their remarks, pieces advice and comments on the manuscript. The authors would like to thank the head of the department of chemistry **Prof. Abdelmonaem TALHAOUI** for making the analytical platform open for the researchers to do all the necessary analyses. We would like also to thank **Mr. ACHALHI Achraf** for his writing assistance, language editing, and proofreading.

Authors contributions:

AN: experimental part, investigation, writing, validation. **EY**: characterization part, investigation, validation. **ER**: investigation, validation. **LM**: theoretical study, writing. **ES**: supervision, formal analysis, correction. **LK**: Formal analysis, data curation, validation. **EA:** supervision, formal analysis, writing-review and editing.

Funding:

This research was partially supported and funded by Mohamed Ist University projects PARA I&II, CNRST and Etelä-Karjala Säästöpankki Foundation, Finland.

Declarations:

Ethics approval:

We declare that there is no financial or personal relationship between us and other people or organizations that may have an inappropriate impact on this work.

Consent to participate:

Consent has been taken from all the authors for participation in this study.

Consent for publication:

Consent has been taken from all the authors for publication of this manuscript.

Conflict of interest:

All authors state that there is no conflict of interest.

Data availability:

The corresponding author will provide the datasets generated for this study on request.

Competing interests:

The authors declare that they have no known competing financial interests or personal relationships that could have appeared to influence the work reported in this paper.

References:

Atmani H, Zazouli S, Bakkardouch FE, Laallam L, Jouaiti A (2021) Insights into interactions of cellulose acetate and metal ions (Zn2+, Cu2+, and Ag+) in aqueous media using DFT study. Computational and Theoretical Chemistry 1202:113322. https://doi.org/10.1016/j.comptc.2021.113322

Banaru AM, Aksenov SM, Banaru DA (2021) Critical Molecular Coordination Numbers in the Structural Class P21/c, Z= 4 (1). Moscow University Chemistry Bulletin 76 (5):325-333. https://doi.org/10.3103/S0027131421050023

Bernard D (1990) An all-electron numerical method for solving the local density functional for polyatomic molecules. The Journal of chemical physics 92 (1):508-517. https://doi.org/10.1063/1.458452

Bernard D (2000) From molecules to solids with the DMol 3 approach. The Journal of chemical physics 113 (18):7756-7764. https://doi.org/10.1063/1.1316015

C.Malaspina D, Faraudo J (2019) Molecular insight into the wetting behavior and amphiphilic character of cellulose nanocrystals. Advances in Colloid and Interface Science 267:15-25. https://doi.org/10.1016/j.cis.2019.02.003

Chauhan GS, Singh B, Dhiman SK (2004) Functionalization of poly (4-vinyl pyridine) grafted cellulose by quaternization reactions and a study on the properties of postquaternized copolymers. journal of applied polymer science 91 (4):2454-2464. https://doi.org/10.1002/app.13406

Chen Q, Peng C, Xie H, Zhao Zk, Bao M (2015) Cellulosic poly (ionic liquid) s: synthesis, characterization and application in the cycloaddition of CO 2 to epoxides. RSC Advances 5 (55):44598-44603. https://doi.org/10.1039/C5RA05667E

Chen Xj, Zhao J, Zhang J, Qiu L, Xu D, Zhang H, Han X, Sun B, Fu G, Zhang Y, Yan F (2012) Bis-imidazolium based poly (ionic liquid) electrolytes for quasi-solid-state dye-sensitized solar cells. Journal of Materials Chemistry 22 (34):18018-18024. https://doi.org/10.1039/C2JM33273F

D.French A (2014) Idealized powder diffraction patterns for cellulose polymorphs. Cellulose 21 (2):885-896. https://doi.org/10.1007/s10570-013-0030-4

Dhopatkar N, Anim-Danso E, Peng C, Singla S, Liu X, Joy A, Dhinojwala A (2018) Reorganization of an amphiphilic glassy polymer surface in contact with water probed by contact angle and sum frequency generation spectroscopy. Macromolecules 51 (14):5114-5120. https://doi.org/10.1021/acs.macromol.8b00640

Du C, Zhang XN, Sun TL, Du M, Zheng Q, Wu ZL (2021) Hydrogen-bond association-mediated dynamics and viscoelastic properties of tough supramolecular hydrogels. Macromolecules 54 (9):4313-4325. https://doi.org/10.1021/acs.macromol.1c00152

El Barkany S, El Idrissi A, Zanagui C, Jilal I, Tabaght F, Abou-Salama M, Amhamdi HJJMES (2017) New branched chain cellulose derivatives based on esparto Stipa tenacissima of eastern Morocco: synthesis and characterization. JMES 8 (4):1195-1210

El Idrissi A, El Barkany S, Amhamdi H, Maaroufi AKJJoaps (2013) Synthesis and characterization of the new cellulose derivative films based on the hydroxyethyl cellulose prepared from esparto “stipa tenacissima” cellulose of Eastern Morocco. II. Esterification with acyl chlorides in a homogeneous medium. journal of applied polymer science 127 (5):3633-3644. https://doi.org/10.1002/app.37982

Fabiano A, Piras AM, Guazzelli L, Storti B, Bizzarri R, Zambito Y (2019) Impact of different mucoadhesive polymeric nanoparticles loaded in thermosensitive hydrogels on transcorneal administration of 5-fluorouracil. Pharmaceutics 11 (12):623. https://doi.org/10.3390/pharmaceutics11120623

Fang Y, Yue T, Li S, Zhang Z, Liu J, Zhang L (2021) Molecular dynamics simulations of self-healing topological copolymers with a comblike structure. Macromolecules 54 (3):1095-1105. https://doi.org/10.1021/acs.macromol.0c02056

Fei P, Liao L, Meng J, Cheng B, Hu X, Song J (2018) Synthesis, characterization and antibacterial properties of reverse osmosis membranes from cellulose bromoacetate. Cellulose 25 (10):5967-5984. https://doi.org/10.1007/s10570-018-1990-1

Freitas RRMd, Senna AM, Botaro VR (2017) Influence of degree of substitution on thermal dynamic mechanical and physicochemical properties of cellulose acetate. Industrial crops and products 109:452-458. https://doi.org/10.1016/j.indcrop.2017.08.062

Frisch M, Trucks G, Schlegel H, Scuseria G, Robb M, Cheeseman J, Scalmani G, Barone V, Mennucci B, Petersson G (2009) Gaussian 09, Revision D. 01, Gaussian, Inc., Wallingford CT. See also: URL: http://www gaussian com

Fu L-H, Qi C, Ma M-G, Wan P (2019) Multifunctional cellulose-based hydrogels for biomedical applications. Journal of Materials Chemistry B 7 (10):1541-1562. https://doi.org/10.1039/C8TB02331J

Ge W, Shuai J, Wang Y, Zhou Y, Wang X (2022) Progress on chemical modification of cellulose in “green” solvents. Polymer Chemistry. https://doi.org/10.1039/D1PY00879J

Gu H, Gao X, Zhang H, Chen K, Peng L (2020) Fabrication and characterization of cellulose nanoparticles from maize stalk pith via ultrasonic-mediated cationic etherification. Ultrason Sonochem 66:104932. https://doi.org/10.1016/j.ultsonch.2019.104932

Guo Y, Zhao C, Yu P, Gao J, Liang Z, Ji R, Du H, Fu J, Liang J, DongYang (2021) Molecular basis of sodium chloride dominated glutenin interaction and bread properties. LWT 142:111011. https://doi.org/10.1016/j.lwt.2021.111011

Hassan AFH, Babin J, Arnal-Herault C, David L, Jonquieres A (2016) Grafting of cellulose acetate with ionic liquids for biofuel purification by a membrane process: Influence of the cation. carbohydrate polymers 147:313-322. https://doi.org/10.1016/j.carbpol.2016.04.008

Heinze T (2015) Cellulose: structure and properties. Cellulose Chemistry and Properties: Fibers, Nanocelluloses and Advanced Materials:1-52. https://doi.org/10.1007/12_2015_319

Holly FJ, Refojo MF (1975) Wettability of hydrogels. I. Poly (2-hydroxyethyl methacrylate). Journal of Biomedical Materials Research 9 (3):315-326. https://doi.org/10.1002/jbm.820090307

Humphrey W, Dalke A, Schulten K (1996) VMD: visual molecular dynamics. Journal of Molecular Graphics 14 (1):33-38, 27-38. https://doi.org/10.1016/0263-7855(96)00018-5

J.Grabowski S (2021) Intramolecular Hydrogen Bond Energy and Its Decomposition—O–H··· O Interactions. Crystals 11 (1):5. https://doi.org/10.3390/cryst11010005

Joubert F, Yeo RP, Sharples GJ, Musa OM, Hodgson DRW, Cameron NR (2015) Preparation of an Antibacterial Poly(ionic liquid) Graft Copolymer of Hydroxyethyl Cellulose. Biomacromolecules 16 (12):3970-3979. https://doi.org/10.1021/acs.biomac.5b01300

Klemm D, Heublein B, Fink H-P, Bohn A (2005) Cellulose: fascinating biopolymer and sustainable raw material. Angew Chem Int Ed Engl 44 (22):3358-3393. https://doi.org/10.1002/anie.200460587

L.Bernard F, B.Duczinski R, F.Rojas M, C.Fialho MC, Carreño LÁ, V.Chaban V, Vecchia FD, Einloft S (2018) Cellulose based poly (ionic liquids): Tuning cation-anion interaction to improve carbon dioxide sorption. Fuel 211:76-86. https://doi.org/10.1016/j.fuel.2017.09.057

Li B, Lu X, Ma Y, Chen Z (2014a) Thermo-and pH-responsive behaviors of aqueous poly (acrylic acid)/poly (4-vinylpyridine) complex material characterized by ATR-FTIR and UV–Vis spectroscopy. European Polymer Journal 60:255-261. https://doi.org/10.1016/j.eurpolymj.2014.09.017

Li F, Wang W, Wang X, Yu J (2014b) Changes of structure and property of alkali soluble hydroxyethyl celluloses (HECs) and their regenerated films with the molar substitution. Carbohydrate polymers 114:206-212. https://doi.org/10.1016/j.carbpol.2014.08.015
Li Y, Gong C, Li C, Ruan K, Liu C, Liu H, Gu J (2021) Liquid crystalline texture and hydrogen bond on the thermal conductivities of intrinsic thermal conductive polymer films. Journal of Materials Science & Technology 82:250-256. https://doi.org/10.1016/j.jmst.2021.01.017
Liu S, J.Edgar K (2017) Water-soluble co-polyelectrolytes by selective modification of cellulose esters. Carbohydrate Polymers 162:1-9. https://doi.org/10.1016/j.carbpol.2017.01.008
Liu S, Liu J, Esker AR, Edgar KJ (2016) An Efficient, Regioselective Pathway to Cationic and Zwitterionic N-Heterocyclic Cellulose Ionomers. Biomacromolecules 17 (2):503-513. https://doi.org/10.1021/acs.biomac.5b01416
Lu T, Chen F (2012) Multiwfn: a multifunctional wavefunction analyzer. Journal of computational chemistry 33 (5):580-592. https://doi.org/10.1002/jcc.22885
Marks JA, Fox SC, Edgar KJ (2016) Cellulosic polyelectrolytes: synthetic pathways to regioselectively substituted ammonium and phosphonium derivatives. Cellulose 23 (3):1687-1704. https://doi.org/10.1007/s10570-016-0929-7
McClements DJ (2006) Non-covalent interactions between proteins and polysaccharides. Biotechnology advances 24 (6):621-625. https://doi.org/10.1016/j.biotechadv.2006.07.003
Mezzetta A, Becherini S, Pretti C, Monni G, Casu V, Chiappe C, Guazzelli L (2019) Insights into the levulinate-based ionic liquid class: Synthesis, cellulose dissolution evaluation and ecotoxicity assessment. New Journal of Chemistry 43 (33):13010-13019. https://doi.org/10.1039/C9NJ03239H
Miao C, Y.Hamad W (2016) Alkenylation of cellulose nanocrystals (CNC) and their applications. Polymer 101:338-346. https://doi.org/10.1016/j.polymer.2016.08.099
Milcovich G, Antunes F, Golob S, Farra R, Grassi M, Voinovich D, Grassi G, Asaro F (2016) Thermo-responsive hydrogels from cellulose-based polyelectrolytes and catanionic vesicles for biomedical application. Journal of Biomedical Materials Research Part A 104 (7):1668-1679. https://doi.org/10.1002/jbm.a.35698
MuzafferTalu, Demiroğlu EU, Yurdakul Ş, Badoğlu S (2015) FTIR, Raman and NMR spectroscopic and DFT theoretical studies on poly (N-vinylimidazole). Spectrochimica Acta Part A: Molecular Biomolecular Spectroscopy 134:267-275. https://doi.org/10.1016/j.saa.2014.06.101
N.Hafiza M, Isa MI (2017) Solid polymer electrolyte production from 2-hydroxyethyl cellulose: Effect of ammonium nitrate composition on its structural properties. Carbohydrate polymers 165:123-131. https://doi.org/10.1016/j.carbpol.2017.02.033
P.Sakellariou, R.C.Rowe (1995) Interactions in cellulose derivative films for oral drug delivery. Progress in polymer science 20 (5):889-942. https://doi.org/10.1016/0079-6700(95)00008-4
Perdew JP, Wang Y (1992) Accurate and simple analytic representation of the electron-gas correlation energy. Physical review B 45 (23):13244. https://doi.org/10.1103/PhysRevB.45.13244
Picart C, Caruso F, Voegel J (2014) Layer-by-layer films for biomedical applications. John Wiley & Sons,
Poulopoulou N, Kasmi N, Bikiaris DN, Papageorgiou DG, Floudas G, Papageorgiou GZ (2018) Sustainable polymers from renewable resources: polymer blends of furan-based polyesters. Macromolecular Materials Engineering 303 (8):1800153. https://doi.org/10.1002/mame.201800153
R.M.Hodge, H.Edward G, P.Simon G (1996) Water absorption and states of water in semicrystalline poly (vinyl alcohol) films. Polymer 37 (8):1371-1376. https://doi.org/10.1016/0032-3861(96)81134-7
Samal SK, Dash M, Vlierberghe SV, Kaplan DL, Chiellini E, Blitterswijk Cv, Moronid L, Dubruel P (2012) Cationic polymers and their therapeutic potential. Chemical Society Reviews 41 (21):7147-7194. https://doi.org/10.1016/0079-6700(95)00008-4
Şen F, Kahraman MV (2018) Preparation and characterization of hybrid cationic hydroxyethyl cellulose/sodium alginate polyelectrolyte antimicrobial films. Polymers for Advanced Technologies 29 (7):1895-1901. https://doi.org/10.1002/pat.4298

Shafiei-Irannejad V, Rahimi M, Zarei M, Dinparast-Isaleh R, Bahrambeigi S, Alihemmati A, Shojaei S, Ghasemi Z, Yousefi B (2019) Polyelectrolyte carboxymethyl cellulose for enhanced delivery of doxorubicin in MCF7 breast cancer cells: Toxicological evaluations in mice model. Pharmaceutical research 36 (5):1-17. https://doi.org/10.1007/s11095-019-2598-3

Shojaeiarani J, Bajwa D, Shirzadifar A (2019) A review on cellulose nanocrystals as promising biocompounds for the synthesis of nanocomposite hydrogels. Carbohydrate Polymers 216:247-259. https://doi.org/10.1016/j.carbpol.2019.04.033

Suna J, Cheng W, Fan W, Wang Y, Meng Z, Zhang S (2009) Reusable and efficient polymer-supported task-specific ionic liquid catalyst for cycloaddition of epoxide with CO2. Catalysis Today 148 (3-4):361-367. https://doi.org/10.1016/j.cattod.2009.07.070

T.Mahmudov K, N.Kopylovich M, Silva MFCGd, J.L.Pombeiro A (2017) Non-covalent interactions in the synthesis of coordination compounds: Recent advances. Coordination Chemistry Reviews 345:54-72. https://doi.org/10.1016/j.ccr.2016.09.002

Thanou M, Verhoef JC, Junginger HE (2001) Oral drug absorption enhancement by chitosan and its derivatives. Advanced drug delivery reviews

52 (2):117-126. https://doi.org/10.1016/S0169-409X(01)00231-9

Trivedi MK, Nayak G, Patil S, Tallapragada RM, Mishra R (2015) Influence of biofield treatment on physicochemical properties of hydroxyethyl cellulose and hydroxypropyl cellulose. Molecular Pharmaceutics Organic Process Research 3 (2). http://dx.doi.org/10.4172/2329-9053.1000126

Tschan MJ-L, Brulé E, Haquette P, Thomas CM (2012) Synthesis of biodegradable polymers from renewable resources. Polymer Chemistry 3 (4):836-851. https://doi.org/10.1039/C2PY00452F

Vasiliu S, Racovita S, Popa M, Ochiuz L, Peptu CA (2019) Chitosan-based polyelectrolyte complex hydrogels for biomedical applications. In: Cellulose-based superabsorbent hydrogels. Springer, pp 1695-1725. doi:https://doi.org/10.1007/978-3-319-77830-3_56

Wang W, Li F, Yu J, Navard P, Budtova T (2015) Structure and properties of novel cellulose-based fibers spun from aqueous NaOH solvent under various drawing conditions. Cellulose 22 (2):1333-1345. https://doi.org/10.1007/s10570-015-0544-z

Watanabe K, Watanabe C, Honma T, Tian Y-S, Kawashima Y, Kawashita N, Takagi T, Fukuzawa K (2021) Intermolecular Interaction Analyses on SARS-CoV-2 Spike Protein Receptor Binding Domain and Human Angiotensin-Converting Enzyme 2 Receptor-Blocking Antibody/Peptide Using Fragment Molecular Orbital Calculation. The journal of physical chemistry letters 12 (16):4059-4066. https://doi.org/10.1021/acs.jpclett.1c00663

Xu Z, Liu Y (2021) The Behavior of Carbonized Polymer Dots at the Nano-Bio Interface and Their Luminescent Mechanism: A Physical Chemistry Perspective. Chinese Journal of Chemistry 39 (2):265-273. https://doi.org/10.1002/cjoc.202000334

Xue Y, Xiao H (2015) Antibacterial/antiviral property and mechanism of dual-functional quaternized pyridinium-type copolymer. Polymers 7 (11):2290-2303. https://doi.org/10.3390/polym7111514

Zhu Y, Romain C, Williams CK (2016) Sustainable polymers from renewable resources. Nature 540 (7633):354-362. https://doi.org/10.1038/nature21001